Hydroxyl tagging velocimetry in a supersonic flow over a cavity

Robert W. Pitz, Michael D. Lahr, Zachary W. Douglas, Joseph A. Wehrmeyer, Shengteng Hu, Campbell D. Carter, Kuang-Yu Hsu, Chee Lum, and Manoochehr M. Koochesfahani

Hydroxyl tagging velocimetry (HTV) measurements of velocity were made in a Mach 2 (M 2) flow with a wall cavity. In the HTV method, ArF excimer laser (193 nm) beams pass through a humid gas and dissociate H_2O into H + OH to form a tagging grid of OH molecules. In this study, a 7×7 grid of hydroxyl (OH) molecules is tracked by planar laser-induced fluorescence. The grid motion over a fixed time delay yields about 50 velocity vectors of the two-dimensional flow in the plane of the laser sheets. Velocity precision is limited by the error in finding the crossing location of the OH lines written by the excimer tag laser. With a signal-to-noise ratio of about 10 for the OH lines, the determination of the crossing location is expected to be accurate within ± 0.1 pixels. Velocity precision within the freestream, where the turbulence is low, is consistent with this error. Instantaneous, single-shot measurements of two-dimensional flow patterns were made in the nonreacting M 2 flow with a wall cavity under low- and high-pressure conditions. The single-shot profiles were analyzed to yield mean and rms velocity profiles in the M 2 nonreacting flow.

OCIS codes: 120.7250, 280.7250, 120.4820, 280.2490, 300.2530, 300.6540.

1. Introduction

Nonintrusive measurements of velocity are needed in supersonic flows, where probes easily produce flow disturbances. Nonintrusive gas-phase velocity measurements are normally made with laser scattering from particles that naturally exist in the flow or are added to the flow. Particle-based velocity methods include techniques such as laser Doppler velocimetry, particle image velocimetry, planar Doppler velocimetry, and phase Doppler anemometry.[1,2] In supersonic flows the particle velocity often differs from the actual gas velocity because of particle drag and a slow response to velocity gradients.[3] Also, in confined flows the particles can coat the windows, leading to limited test times or even window abrasion.[4]

Unlike particle-based methods, laser-based molecular velocity methods directly measure the gas velocity. In Doppler-shift methods, the small Doppler shift is measured and related to the velocity. These methods are more accurate at higher velocities, as the Doppler shift is larger and more easily measured, but they often yield only average flow velocities owing to a lack of signal strength. Many of these Doppler-based molecular velocity methods are based on laser-induced fluorescence of molecules (or atoms) that are added to the flows such as copper,[5] hydroxyl,[6,7] nitric oxide,[8] sodium,[9] and iodine.[10] The addition of such species is often impractical in test facilities. Also, in Doppler-shift methods the optical geometry of the laser and the observer define the velocity component that is measured, and this feature can be limiting.[11] Other Doppler-shift velocity methods are based on Rayleigh scattering from the gas molecules,[12,13] but Rayleigh scattering signals are weak and are difficult to obtain in confined facilities because of interference from laser scattering from the walls and particles in the flow.[11]

Molecular tagging methods yield the gas velocity by time of flight; the molecules in the gas flow are tagged or marked with a laser, and the movement of

R. W. Pitz (robert.w.pitz@vanderbilt.edu), M. D. Lahr (michael.d.lahr@vanderbilt.edu), Z. W. Douglas (zachary.w.douglas@vanderbilt.edu), J. A. Wehrmeyer, and S. Hu are with the Department of Mechanical Engineering, Vanderbilt University, Nashville, Tennessee 37235. C. D. Carter is with the Air Force Research Laboratory (AFL/PRAS), Wright-Patterson Air Force Base, Ohio 45433; K.-Y. Hsu is with Innovative Scientific Solutions, Inc., Dayton, Ohio 45440; C. Lum and M. M. Koochesfahani are with the Department of Mechanical Engineering, Michigan State University, East Lansing, Michigan 48824.

Received 7 February 2005; revised manuscript received 19 May 2005; accepted 17 March 2005.

0003-6935/05/316692-09$15.00/0

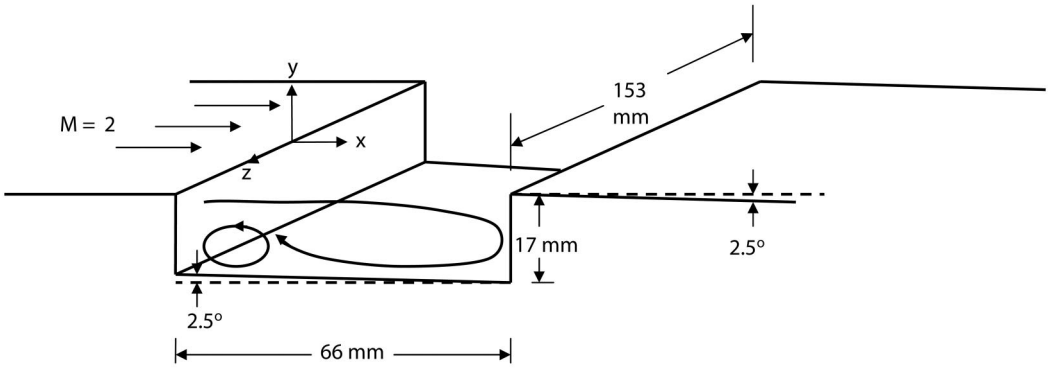

Fig. 1. Mach 2 cavity-piloted flow.

the tag gives the velocity. Once a laser line or grid is tagged, the grid will move with the flow. The movement of the tagged regions is imaged by a method dictated by the photochemistry of the tagged molecules (laser-induced fluorescence in the case of hydroxyl tagging velocimetry, HTV). The displacement of the tagged grid over a fixed time period yields the velocity.

Many molecular tagging methods use a gas seed. A gas molecule (or atom) is added to the flow and the molecule is tagged with a laser beam (e.g., electronically excited, photodissociated, or vibrationally excited). In gas-seeded methods, the flow is seeded with molecules (or atoms) such as acetone,[14] biacetyl,[15,16] nitric oxide,[11,17] nitrogen dioxide,[18] sodium,[19] strontium[20] or *tert*-butyl nitrate.[21] For test facility flows, the addition of these atomic or molecular seeds is often undesirable for to a variety of reasons (seed toxicity, expense, etc.).

There are unseeded tagging methods in which gas tags are produced from molecules naturally occurring in air (i.e., nitrogen, oxygen, water vapor). Examples of molecular tags produced from air are N_2^+ ion,[22] ozone,[23–25] hydroxyl,[25–30] nitric oxide,[31–33] and vibrationally excited oxygen.[13,34] Many of the methods use nonlinear laser excitation[13,22,26,31–34] to produce these tags from air, and the tag is produced only in a small region near the laser focus. In the present work, HTV is used, which is a linear method.[28–30] An ArF laser at 193 nm photodissociates water in a single-photon process to produce OH in a grid. The OH grid moves for a known period of time, and the position of the grid is recorded with laser-induced fluorescence of OH.

Accurate nonintrusive velocity data are limited in high-speed, compressible flows, in part because of biasing effects when conventional particle-based laser velocity methods are applied.[3] Nonintrusive ve-

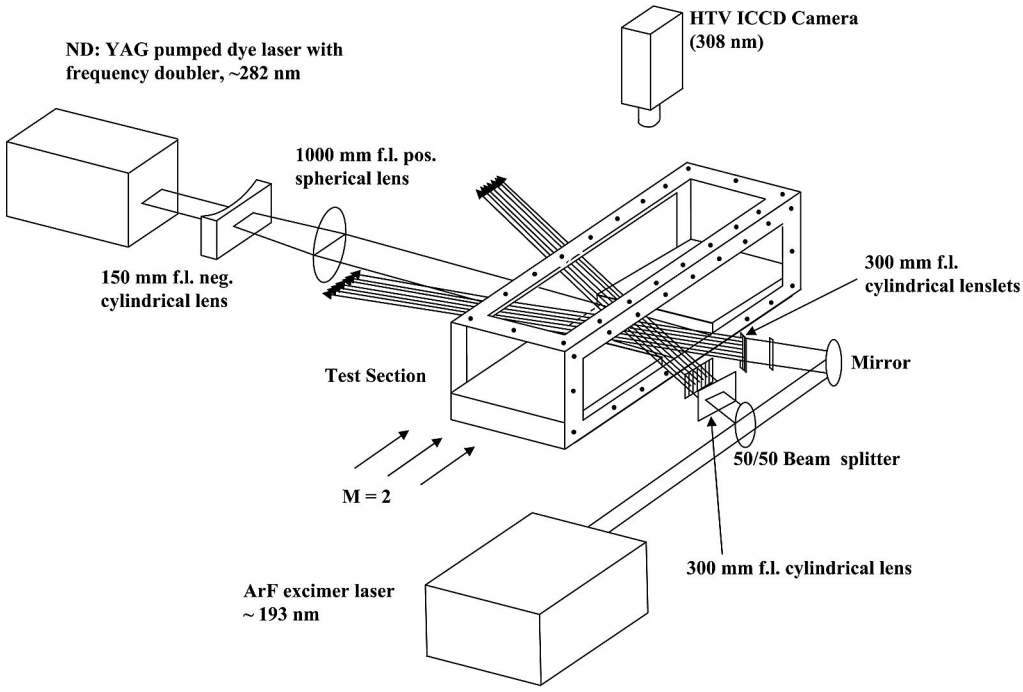

Fig. 2. Schematic of the HTV experimental system; f.l., focal length; M, Mach.

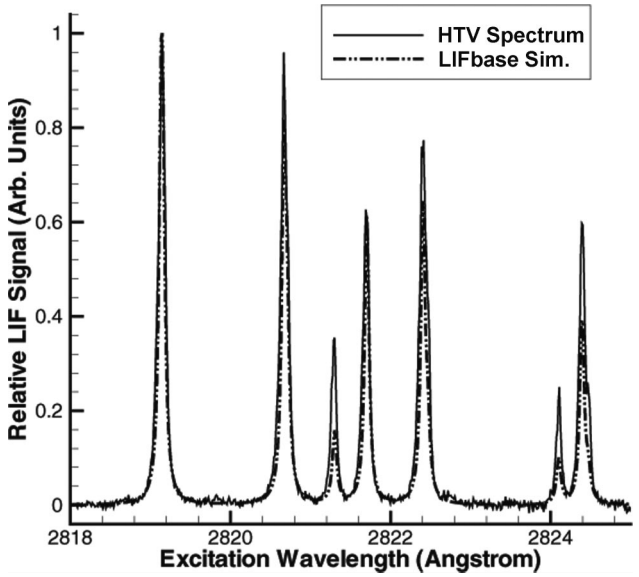

Fig. 3. Experimental and simulated excitation scans (relative to the $Q_1(1)$ signal) across OH A–$X(1, 0)$ transitions. Broadening of the simulated spectrum (temperature $T = 295$ K, LIFbase version 2) was adjusted to match the experimental spectrum approximately; peak heights of the experimental and simulated $Q_1(1) + R_2(3)$ line were also matched. The experimental spectrum was derived from a sequence of 600 images, each image being the sum of 5 exposures of the grid at ~295 K and 745 Torr.

locity data are needed in flows relevant to scramjet combustion, and molecular-based methods such as HTV avoid the problems associated with particle-based methods. In scramjets, wall cavities are commonly used to stabilize combustion with minimal pressure drag.[35] An optically accessible supersonic flow facility has been developed to study cavity-stabilized supersonic reacting flows, and to compare the results with advanced computational fluid dynamics models.[36–38] In this work the HTV method is applied to a Mach 2 (M 2) flow with a wall cavity to obtain instantaneous two-dimensional velocity images, mean velocity profiles, and rms velocity profiles. Velocity measurements are made by using HTV in the freestream (over the cavity) and within the cavity of the M 2 cavity-piloted combustor.

2. Experimental System

The experiments were conducted at the supersonic flow facility in Research Cell 19 at the Air Force Research Laboratory, Propulsion Directorate at Wright-Patterson Air Force Base. The tunnel has a two-dimensional M 2 nozzle. The air flow rate was about 1.4 kg/s. A schematic of the test configuration is shown in Fig. 1. Fused-silica windows (Suprasil, with good transmission at 193 nm) form the side walls of the tunnel. The tunnel has a constant-area isolator section upstream of the cavity with a cross section of 51 mm high by 153 mm wide; downstream of the isolator, the bottom wall diverges at an angle of 2.5°. A cavity to provide a flame pilot forms the bottom surface of the tunnel, as shown in Fig. 1. The cavity is 17 mm deep and 66 mm long. A shear layer forms at the edge of the first step in the cavity, and the recirculation zone is produced by the cavity.

A schematic of the HTV system is shown in Fig. 2. A Lambda Physik Compex 150T ArF excimer laser was used to produce a 193 nm laser beam. The ArF excimer laser beam (20 mm high by 10 mm wide, 115 mJ/pulse, broadband, 1 nm bandwidth) was split into two beams by a beam splitter. Each of the laser beams was sent through grid-forming optics that produce two sets of seven beams each. The grid optics consist of two major components placed very close together: a 300 mm focal length cylindrical lens (25 mm × 40 mm) and a stack of 300 mm cylindrical lenses (20 mm wide by 3 mm high). The beam diameter was about 0.3 mm in the measurement zone. The sets of beams produce 49 crossing points in the measurement zone. The energies for the two sets of beams before transmission into the tunnel were measured at 20 mJ on the 2.3 m beam path (left grid) and 10 mJ on the 3.0 m beam path (right grid). With the ArF excimer laser operating broadband instead of narrowband, much of the beam was absorbed by O_2 (about 85%) before the beams crossed in the measurement zone: in principle, the laser can be tuned to avoid O_2 transitions, thereby improving beam transmission to the tunnel. This increase in energy can improve grid imaging and improve the postprocessing by increasing the signal-to-noise ratio.

The 7 × 7 grid of ArF-generated lines of OH was imaged by laser-induced fluorescence of OH by using the $Q_1(1)$ transition of the $A^2\Sigma^+$ $(v' = 1) \leftarrow X^2\Pi_i$ $(v'' = 0)$ band at 282 nm. A Spectra Physics Model GRC 170 Nd:YAG laser (injection seeded) pumped a Lumonics HD-300 Hyperdye dye laser. The output of the dye laser was doubled by an Inrad Autotracker II to produce about 20 mJ/pulse of 282 nm laser radiation. A small portion of the 282 nm beam was split off and directed over a small flame and then to a photodiode. Signals from the photodiode and a photomultiplier tube—recording the OH laser-induced

Table 1. Mach 2 Flow with a Wall Cavity

Test	Stagnation Conditions		Isentropic Conditions Mach 2		Air Mass Flow Rate (kg/sec)	Water Mass Flow Rate (g/sec)	Back Pressure Valve (%)	Cavity Bottom Wall Pressure (kPa)
	P_0 (kPa)	T_0 (K)	P (kPa)	T (K)				
A	170	520	22	290	1.4	25	0	35
B	170	520	22	290	1.4	25	64	70

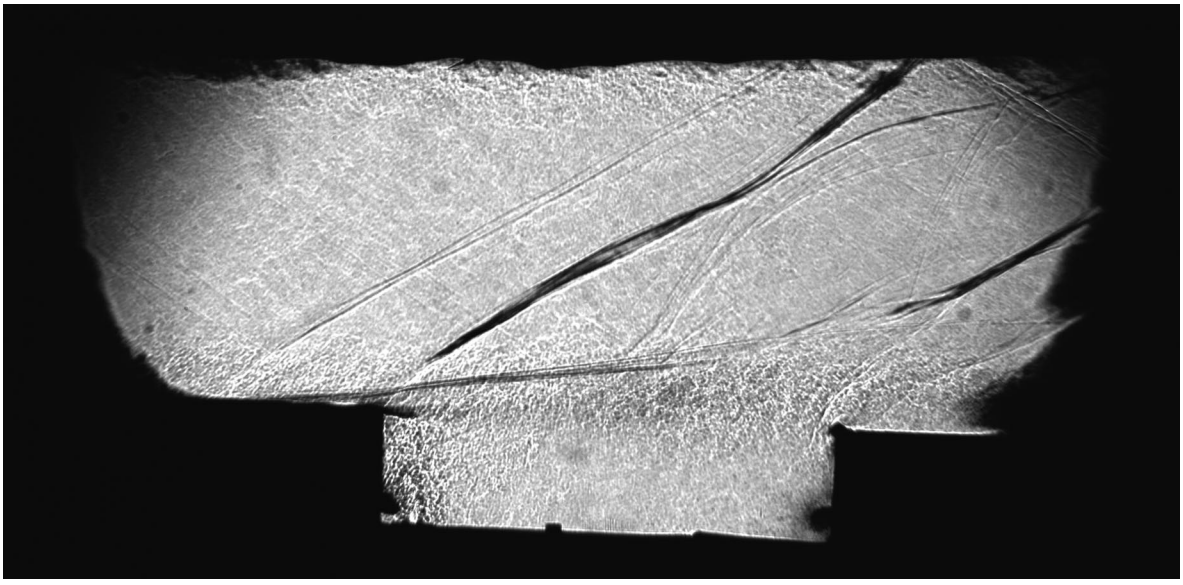

Fig. 4. Shadowgraph single-shot image over a rectangular cavity in a M 2 nonreacting cavity flow under low-backpressure conditions (flow is from left to right).

fluorescence from the flame—were displayed on an oscilloscope to ensure proper operation of the dye laser and good overlap with the OH transition. Timing of the lasers and camera was accomplished with a Quantum Composer (model 9318E) pulse generator. Random (shot-to-shot) timing error between the lasers was about ±20 ns, or about ±1% of the typical 2 μs timing separation.

The OH-probe laser beam was expanded by a negative cylindrical lens (focal length −150 mm) and focused by a 1000 mm focal length spherical lens to form a sheet. To improve the signal strength, the laser sheet was retroreflected through the tunnel, with a delay of about 5 ns. Both this sheet and the 193 nm grid were rotated to be parallel to the tunnel bottom floor (2.5° off the horizontal plane).

Fluorescence from the created OH was recorded with a PIMAX Superblue intensified CCD camera, which was fitted with a 45-mm $f/1.8$ UV lens (Cerco). Schott glass filters (WG-295 or 305 and UG-11) were employed to block background scattering and fluorescence (from tunnel surfaces). Typically, the 512 × 512 pixel array of the PIMAX camera was binned 2 × 2 to improve the signal strength. The field of view was 40 mm square, and the camera looked down on the cavity through the tunnel top window (also made of Suprasil). Each 2 × 2 binned pixel imaged a 156 μm × 156 μm region of the flow field. The region probed was roughly in the spanwise center of the flow field and over or within the cavity, as noted above.

Focusing optics (for both laser systems) and the ICCD camera were mounted on a three-dimensional traversing table located beneath the tunnel; the la-

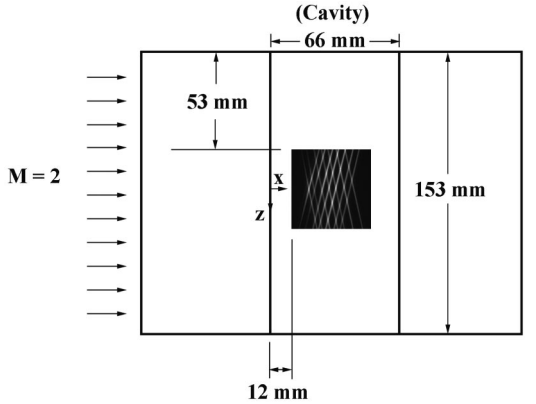

Fig. 5. Overhead schematic of the cavity, showing the position of the HTV images with regard to the cavity steps and test section walls.

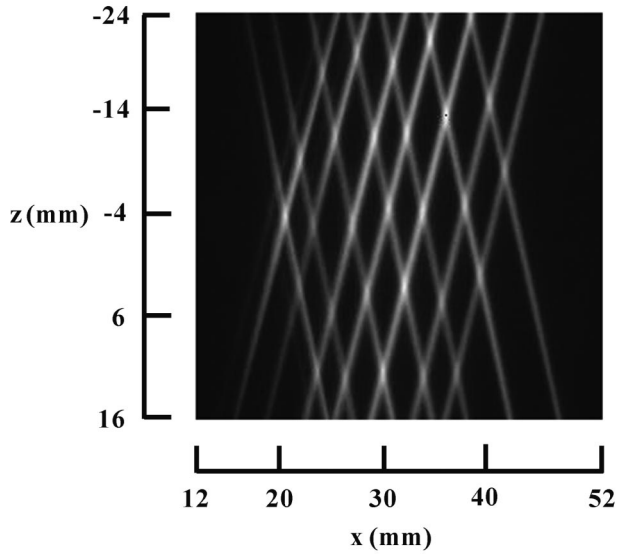

Fig. 6. Averaged undelayed HTV image (at $y = 15.65$ mm, where $z = 0$ is the centerline of the cavity and $x = 0$ is at the front face of the cavity).

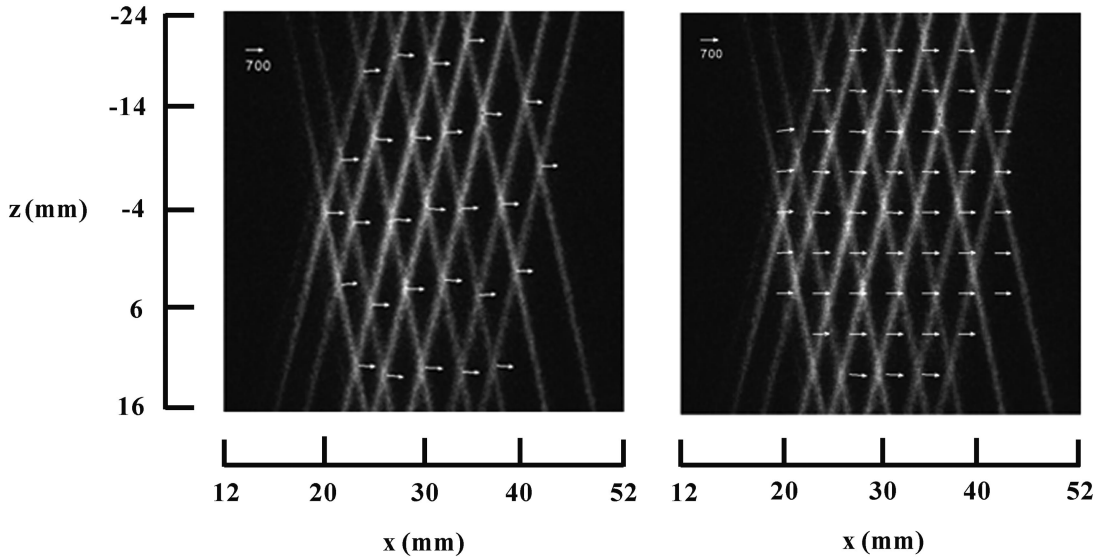

Fig. 7. Single-shot HTV images, giving velocity fields with (left) an irregular and (right) a regular grid in a M 2 nonreacting scramjet cavity flow under a low-backpressure conditions (at $y = 15.65$ mm, where $z = 0$ is the centerline of the cavity and $x = 0$ is at the front face of the cavity).

sers, however, were not mounted on this table. The optics between the lasers and traversing table were thus arranged to allow the laser grid and sheet height location to be varied and thus the shear layer and cavity to be probed.

With stagnant room air in the tunnel at ambient pressure, the ArF excimer laser was pulsed to create the OH grid that was subsequently excited by the OH-probe laser sheet after a short delay ($\sim$0.2 μs). The laser-induced fluorescence (LIF) signal was recorded by the ICCD camera, and the OH probe laser wavelength was scanned over about 0.7 nm. The resultant laser excitation scan is shown in Fig. 3. The measured spectrum was compared with a simulated spectrum calculated by LIFbase[39] (version 2). The measured and calculated line positions match very well. At room temperature (295 K) the strongest line is the combined $Q_1(1) + R_2(3)$ peak in the OH A–$X(1, 0)$ band. Thus the OH probe laser was tuned to this line for a maximum signal. It is worth noting that transition saturation effects distort the spectrum, thus preventing the spectrum from being adequately fitted by simulated spectra.

3. Results

HTV measurements were made in air with no fuel addition. The conditions for the nonreacting flow are given in Table 1. Test A is the low-backpressure condition, where the backpressure valve downstream of the test section is fully open. Test B is the high-

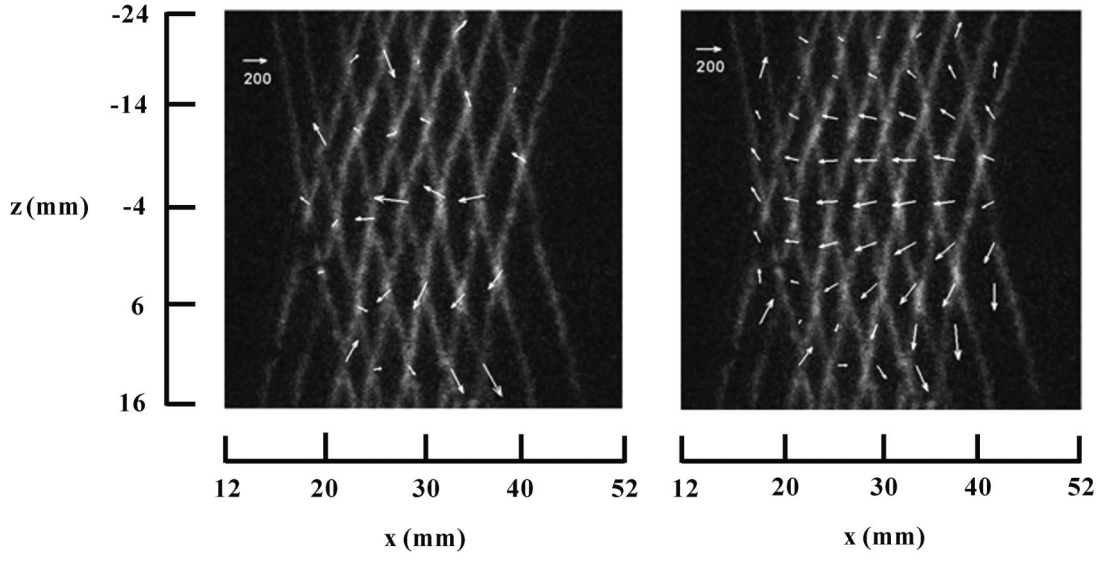

Fig. 8. Single-shot HTV images, giving velocity fields with (left) an irregular and (right) a regular grid in a M 2 nonreacting scramjet cavity flow under low-backpressure conditions (at $y = -4.67$ mm, where $z = 0$ is the centerline of the cavity and $x = 0$ is at the front face of the cavity).

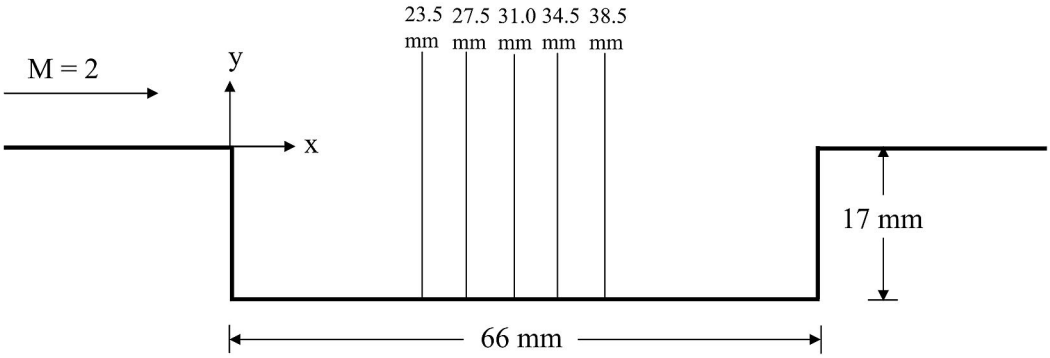

Fig. 9. Side-view schematic of the cavity, showing the profile locations along the x axis.

backpressure condition, where the backpressure valve is 64% closed. The high-backpressure condition simulates the pressure rise from main-duct combustion. Under low-backpressure conditions the tunnel flow above the cavity is largely free of shock waves. A shadowgraph single-shot image (200 μs exposure) of the M 2, nonreacting flow under low-backpressure conditions is shown in Fig. 4.[40] Under high-backpressure conditions strong shocks appear above the cavity, causing the shear layer to be deflected upward (see Fig. 2 of Ref. 38).

Since the tunnel air was dried, water was sprayed into the stagnation chamber to provide moist air and adequate OH planar laser-induced fluorescence signal levels. Sufficient water was added to increase the relative humidity at M 2 isentropic conditions to about 32% (P = 22 kPa, T = 290 K). HTV measurements were made in the spanwise direction in the tunnel. The position of the measured OH grids with regard to the cavity walls is shown in Fig. 5. Examples of two-dimensional instantaneous velocity images from the HTV method are shown in Figs. 6, 7, and 8. Figure 6 is an example of an undelayed averaged HTV image used as the reference for the displaced grid patterns. The velocity vectors in Figs. 7 and 8 are shown on top of the displaced HTV grid pattern. The displacement of each grid intersection is determined by a direct digital spatial correlation technique by using an in-house code.[41] A small region surrounding a grid intersection in the undelayed image, referred to as the source window, is spatially correlated with a larger roam window in the delayed image. The location of the peak of the correlation coefficient is identified as the displacement vector, which after division by the time delay between the two images provides the estimate of the spatial average of the velocity within the source window. Subpixel accuracy is achieved by using a multidimensional polynomial fit to the region near the correlation peak. The details of this procedure and its performance are described by Gendrich and Koochesfahani.[41] In this work the time delay is either 2 or 3 μs. For the low-backpressure condition a delay of 2 μs was used for y = 15.65 mm to y = 0.41 mm, while a 3 μs delay was used for y = −2.13 mm to y = −12.3 mm. For the high-backpressure condition a delay of 2 μs was used for y = 15.65 mm to y = −2.13 mm, and a delay of 3 μs was used for y = −4.67 mm to y = −12.3 mm.

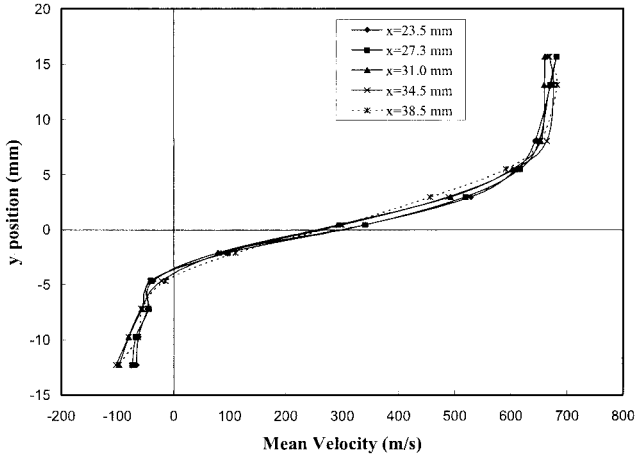

Fig. 10. Mean velocity profiles at various streamwise (x) locations, showing the shear layer between the freestream and the cavity under low-backpressure conditions. (Near centerline, z = −3.5 mm, where z = 0 is the centerline of the cavity and x = 0 is at the front face of the cavity).

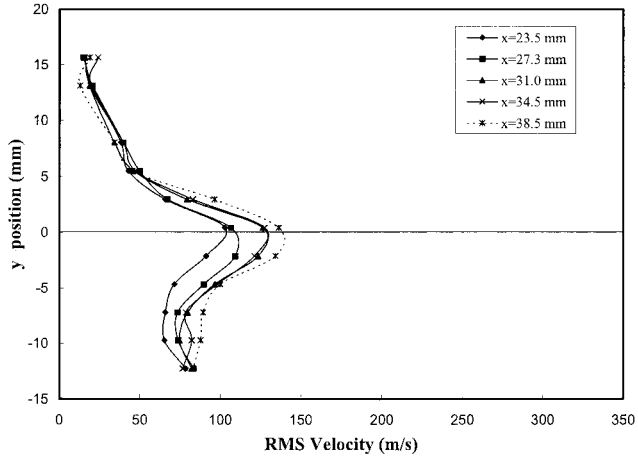

Fig. 11. Rms velocity profiles at various streamwise (x) locations, showing the shear layer between the freestream and the cavity under low-backpressure conditions. (Near centerline, z = −3.5 mm, where z = 0 is the centerline of the cavity and x = 0 is at the front face of the cavity).

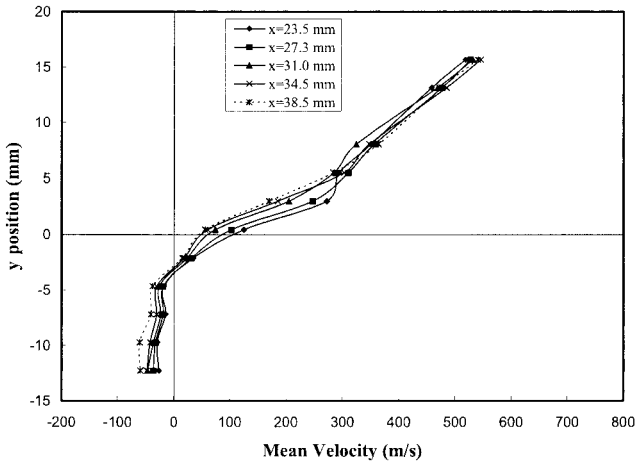

Fig. 12. Mean velocity profiles at various streamwise (x) locations, showing the shear layer between the freestream and the cavity under high-backpressure conditions. (Near centerline, $z = -3.5$ mm, where $z = 0$ is the centerline of the cavity and $x = 0$ is at the front face of the cavity).

The HTV data is obtained originally on an irregularly spaced measurement grid. To take advantage of standard data display and processing techniques, the MTV data is remapped onto a grid with uniform spacing. The remapping is done by using a local least-squares fit to a two-dimensional second-order polynomial. The irregular grid and regular grid spacing applied to the HTV measurements are shown in Figs. 7 and 8. The irregular grid pattern shown on the left is fitted by this procedure onto the regular grid shown on the right. The details of the procedure and its performance characteristics are given by Cohn and Koochesfahani.[42]

In the freestream above the cavity shown in Fig. 7, the velocity pattern is very uniform with a value of about 680 m/s (note the reference vector of 700 m/s). The higher velocity (higher than expected for the M 2 nozzle) arises from the divergence of the bottom wall. In the cavity the flow reverses, and the velocity pattern is much more variable, as is seen in Fig. 8. The velocities in the cavity are reversed with a negative velocity of up to about 200 m/s (note reference vector of 200 m/s).

The average signal-to-noise ratio of the single-shot images is about 7–13. With a crossing angle of about 150°, the center of the line crossings can be determined within 0.1 pixels or a displacement uncertainty of ± 16 μm according to previous calculations (see Fig. 5 of Ref. 41). Thus the uncertainty of the velocity measurement due to the crossing-point determination is about 8 m/s for a 2 μs delay or 5 m/s for a 3 μs delay. Thus with this technique one can achieve comparable relative uncertainty—about $\pm 1\%$ for the full-scale displacement—to that with the particle image velocimetry technique (which is limited in a similar fashion by correlation peak-finding uncertainty).

The instantaneous velocity images were analyzed to obtain mean and rms velocity profiles at the locations shown in Fig. 9. The mean velocity profiles at various streamwise (x axis) locations for the low-backpressure case are shown in Fig. 10. Each data point is an average of 100 instantaneous values obtained from the images. Streamwise profiles are shown near the centerline of the tunnel from the freestream to down in the cavity. The average velocities above the cavity are about 680 m/s and decrease in the shear layer and become negative (about −60 m/s) in the cavity. The shear layer profile appears typical of flows formed behind a rearward-facing step.[43] The shear layer width grows with downstream distance, as expected.

The rms velocities for the low-backpressure case are shown in Fig. 11. The rms values in the freestream are as low as 15 m/s, or about 2.2%. This rms value is due to a combination of freestream turbulence and measurement precision. Recall that the timing error is about $\pm 1\%$ of the typical 2 μs delay and the distance error is about 16 μm, equaling 8 m/s or about 1.2%; of course, the timing error could be largely eliminated by recording the timing for each image with a photodiode. The rms values increase in the shear layer and decrease slightly in the cavity, similar to what is observed in the flow behind a rearward-facing step.[43]

The mean and rms values for the high-backpressure case are shown in Figs. 12 and 13. The profiles are drastically changed from the low-backpressure case. Shock waves observed previously[38] greatly modify the mean and rms values of the velocity. These profiles do not correspond to those seen in subsonic flows behind a rearward-facing step.[43] In this unsteady compressible flow with shocks, the shear layer is deflected upward.[38] This results in a mean velocity profile that appears almost linear above the cavity. The rms values are highest above the cavity, where shocks have been previously observed (see Fig. 2 of Ref. 38).

Mean and rms velocity profiles at various spanwise (z axis) locations (see Fig. 14) for the low-

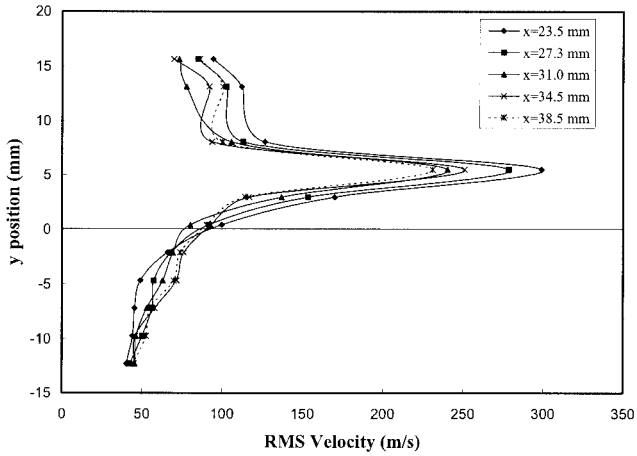

Fig. 13. Rms velocity profiles at various streamwise (x) locations, showing the shear layer between the freestream and the cavity under high-backpressure conditions. (Near centerline, $z = -3.5$ mm, where $z = 0$ is the centerline of the cavity and $x = 0$ is at the front face of the cavity).

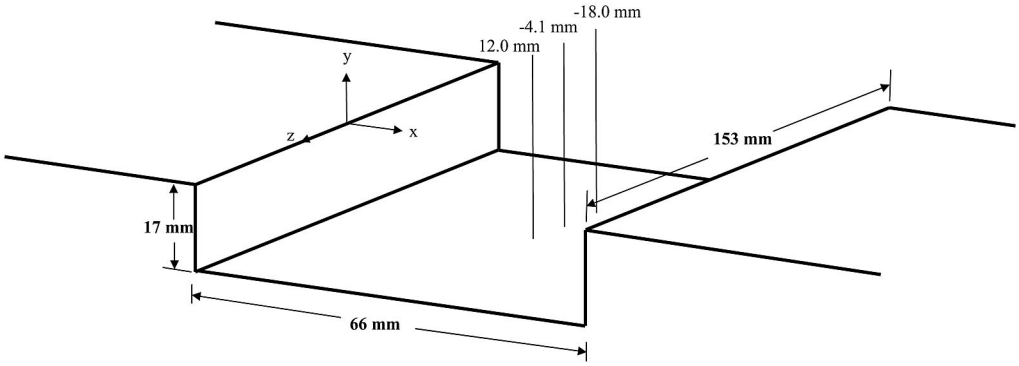

Fig. 14. Schematic of the cavity, showing the profile locations along the z axis.

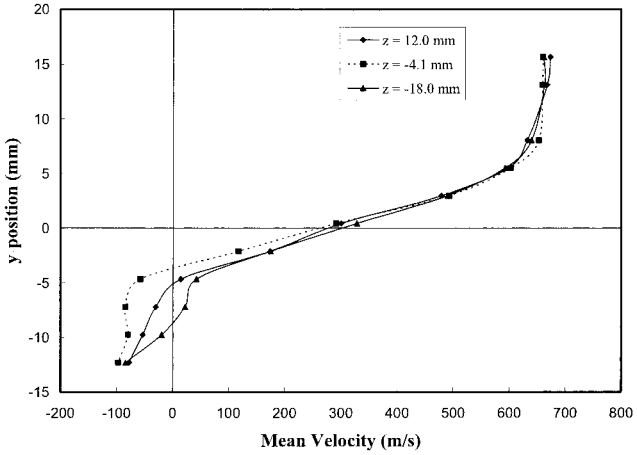

Fig. 15. Mean velocity profiles at three spanwise (z) locations, showing the flow uniformity between the freestream and the cavity under low-backpressure conditions. (Approximately, $x = 31$ mm; $x = 0$ is the front face of the cavity, and $z = 0$ is the centerline of the cavity).

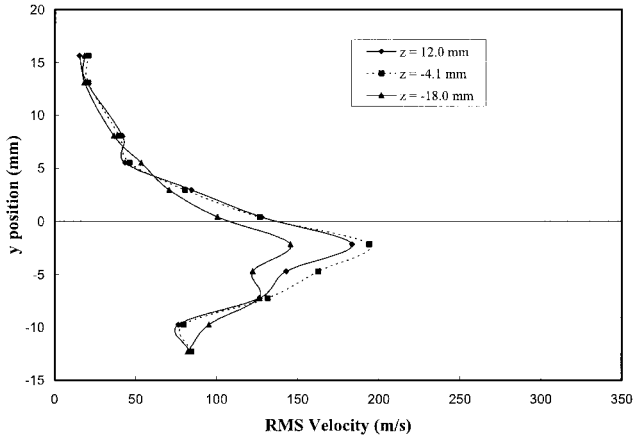

Fig. 16. Rms velocity profiles at three spanwise (z) locations, showing the flow uniformity between the freestream and the cavity under low-backpressure conditions. (Approximately, $x = 31$ mm, where $x = 0$ is the front face of the cavity and $z = 0$ is the centerline of the cavity).

backpressure case are shown in Figs. 15 and 16. The x component (streamwise) of the velocity is uniform in the spanwise direction with vertical location from the freestream to the shear layer as seen in Fig. 15. However, at about $y = -5$ mm the velocity field becomes less uniform in the spanwise direction with the rms velocity rising to almost 200 m/s before the flow regains spanwise uniformity at the bottom of the cavity ($y = -13$ mm). As shown in Figs. 8 and 15, the greatest recirculation occurs around the center of the grid ($z = -4.1$ mm) and decreases away from the centerline.

4. Conclusions

Nonintrusive measurements of velocity were obtained in a M 2 flow with a wall cavity by using hydroxyl tagging velocimetry (HTV) under low- and high-backpressure conditions. Instantaneous two-dimensional images were obtained in the freestream and the cavity. The instantaneous planar measurements were analyzed to determine the mean and rms velocities in the streamwise direction. The rms values of the velocities in the freestream of the M 2 flow are low, consistent with the expected low turbulence values within the freestream and the OH line crossing-point uncertainty equal to or better than 0.1 pixels. Under high-backpressure conditions the shocks in the cavity greatly modify the mean velocity profiles and greatly increase the rms velocity values. These measurements demonstrate the utility of the hydroxyl tagging method. Here, with only the addition of water to the flow, high-fidelity measurements of the velocity field of a high-speed flow above a recessed cavity are possible. Difficulties encountered with particle-based methods—especially in recirculation regions around high-speed core flows—are obviated with this approach. Future work will explore in detail approaches to making measurements in reacting cavities (with high-speed cross flows) and the use of a greater number of grids (e.g., 10×10 and 12×12) to increase the vector density.

This research was supported by the Air Force Office of Scientific Research (AFOSR) under the support of J. Tishkoff. R. W. Pitz was supported by an AFOSR Summer Faculty Fellowship and Arnold Engineering Development Center under contract F40600-03-D-0001. The authors also thank D. Schommer and W. Terry for their technical support.

References

1. R. J. Adrian, "Particle-imaging techniques for experimental fluid mechanics," Annu. Rev. Fluid Mech. **23,** 261–304 (1991).
2. L. E. Drain, *The Laser Doppler Technique* (Wiley, 1980).
3. M. S. Maurice, "Laser velocimetry seed particles within compressible, vertical flows," AIAA J. **30,** 376–383 (1992).
4. R. J. Santoro, S. Pal, R. D. Woodward, and L. Schaaf, "Rocket testing at university facilities," paper AIAA-2001-0748, presented at the 39th AIAA Aerospace Sciences Meeting, Reno, Nev., 8–11 January 2001 (American Institute of Aeronautics and Astronautics, Reston, VA., 2001).
5. W. J. Marinelli, W. J. Kessler, M. G. Allen, S. J. Davis, and S. Arepalli (1991) "Copper atom based measurements of velocity and turbulence in arc jet flows," presented at the 29th AIAA Aerospace Sciences Meeting, Reno, Nev. (American Institute of Aeronautics and Astronautics, 7–10 January 1991, paper AIAA-91-0358.
6. M. Allen, S. Davis, W. Kessler, H. Legner, K. McManus, P. Mulhall, T. Parker, and D. Sonnenfroh, "Velocity field imaging in supersonic reacting flows near atmospheric pressure," AIAA J. **32,** 1676–1682 (1994).
7. K. G. Klavuhn, G. Gauba, and J. C. McDaniel "OH laser-induced fluorescence velocimetry technique for steady, high-speed, reacting flows," J. Propul. Power **10,** 787–797 (1994).
8. P. H. Paul, M. P. Lee, and R. K. Hanson, "Molecular velocity imaging of supersonic flows using pulsed planar laser-induced fluorescence of NO," Opt. Lett. **14,** 417–419 (1989).
9. M. Zimmermann and R. B. Miles, "Hypersonic-helium-flow-field measurements with the resonant Doppler velocimeter," Appl. Phys. Lett. **37,** 885–887 (1980).
10. J. C. McDaniel, B. Hiller, and R. K. Hanson, "Simultaneous multiple-point velocity measurements using laser-induced iodine fluorescence," Opt. Lett. **8,** 51–53 (1983).
11. A. F. P. Houwing, D. R. Smith, J. S. Fox, P. M. Danehy, and N. R. Mudford, "Laminar boundary layer separation at a fin-body junction in a hypersonic flow," Shock Waves **11,** 31–42 (2001).
12. R. G. Seasholtz, F. J. Zupanc, and S. J. Schneider, "Spectrally resolved Rayleigh scattering diagnostic for hydrogen-oxygen rocket plume studies," J. Propul. Power **8,** 935–942 (1992).
13. R. B. Miles and W. R. Lempert, "Quantitative flow visualization in unseeded flows," Annu. Rev. Fluid Mech. **29,** 285–326 (1997).
14. W. R. Lempert, N. Jiang, S. Sethuram, and M. Samimy, "Molecular tagging velocimetry measurements in supersonic microjets," AIAA J. **40,** 1065–1070 (2002).
15. B. Hiller, R. A. Booman, C. Hassa, and R. K. Hanson, "Velocity visualization in gas flows using laser-induced phosphorescence of biacetyl," Rev. Sci. Instrum. **55,** 1964–1967 (1984).
16. B. Stier and M. M. Koochesfahani, "Molecular tagging velocimetry (MTV) measurements in gas phase flows," Exp. Fluids **26,** 297–304 (1999).
17. P. M. Danehy, S. O'Byrne, A. F. P. Houwing, J. S. Fox, and D. R. Smith, "Flow-tagging velocimetry for hypersonic flows using fluorescence of nitric oxide," AIAA J. **41,** 263–271 (2003).
18. C. Orlemann, C. Schulz, and J. Wolfrum, "NO-flow tagging by photodissociation of NO_2. A new approach for measuring small-scale flow structures," Chem. Phys. Lett. **307,** 15–20 (1999).
19. P. Barker, A. Thomas, H. Rubinsztein-Dunlop, and P. Ljungberg, "Velocity measurements by flow tagging employing laser enhanced ionisation and laser induced fluorescence," Spectrochim. Acta B **50,** 1301–1310 (1995).
20. H. Rubinzstein-Dunlop, B. Littleton, P. Barker, P. Ljungberg, and Y. Malmsten, "Ionic strontium fluorescence as a method for flow tagging velocimetry," Exp. Fluids **30,** 36–42 (2001).
21. S. Krüger and G. Grünefeld, "Stereoscopic flow-tagging velocimetry," Appl. Phys. B **69,** 509–512 (1999).
22. J. M. Ress, G. Laufer, and R. H. Krauss, "Laser ion time-of-flight velocity measurements using N_2^+ tracers," AIAA J. **33,** 296–301 (1995).
23. R. W. Pitz, T. M. Brown, S. P. Nandula, P. A. Skaggs, P. A. DeBarber, M. S. Brown, and J. Segall, "Unseeded velocity measurement by ozone tagging velocimetry," Opt. Lett. **21,** 755–757 (1996).
24. L. A. Ribarov, J. A. Wehrmeyer, F. Batliwala, R. W. Pitz, and P. A. DeBarber, "Ozone tagging velocimetry using narrowband excimer lasers," AIAA J. **37,** 708–714 (1999).
25. R. W. Pitz, J. A. Wehrmeyer, L. A. Ribarov, D. A. Oguss, F. Batliwala, P. A. DeBarber, S. Deusch, and P. E. Dimotakis, "Unseeded molecular flow tagging in cold and hot flows using ozone and hydroxyl tagging velocimetry," Meas. Sci. Tech. **11,** 1259–1271 (2000).
26. L. R. Boedeker, "Velocity measurement by H_2O photolysis and laser-induced fluorescence of OH," Opt. Lett. **14,** 473–475 (1989).
27. D. F. Davidson, A. Y. Chang, M. D. DiRosa, and R. K. Hanson, "Continuous wave laser absorption techniques for gas dynamic measurements in supersonic flows," Appl. Opt. **30,** 2598–2608 (1991).
28. J. A. Wehrmeyer, L. A. Ribarov, D. A. Oguss, and R. W. Pitz, "Flame flow tagging velocimetry with 193-nm H_2O photodissociation," Appl. Opt. **38,** 6912–6917 (1999).
29. L. A. Ribarov, J. A. Wehrmeyer, R. W. Pitz, and R. A. Yetter, "Hydroxyl tagging velocimetry (HTV) in experimental air flows," App. Phys. B **74,** 175–183 (2002).
30. L. A. Ribarov, J. A. Wehrmeyer, S. Hu, and R. W. Pitz, "Multiline hydroxyl tagging velocimetry measurements in reacting and nonreacting experimental flows," Exp. Fluids **37,** 65–74 (2004).
31. N. Dam, R. J. H. Klein-Douwel, N. M. Sijtsema, and J. J. ter Meulen, "Nitric oxide flow tagging in unseeded air," Opt. Lett. **26,** 36–38 (2001).
32. N. M. Sijtsema, N. J. Dam, R. J. H. Klein-Douwel, and J. J. ter Meulen, "Air photolysis and recombination tracking: A new molecular tagging velocimetry scheme," AIAA J. **40,** 1061–1064 (2002).
33. W. P. N. van der Laan, R. A. L. Tolboom, N. J. Dam, and J. J. ter Meulen, "Molecular tagging velocimetry in the wake of an object in supersonic flow," Exp. Fluid **34,** 531–533 (2003).
34. A. Noullez, G. Wallace, W. Lempert, R. B. Miles, and U. Frisch, "Transverse velocity increments in turbulent flow using the RELIEF technique," J. Fluid Mech. **339,** 287–307 (1997).
35. A. Ben-Yakar and R. K. Hanson, "Cavity flame-holders for ignition and flame stabilization in scramjets: an overview," J. Propul. Power **17,** 869–877 (2001).
36. M. R. Gruber and A. S. Nejad, "New supersonic combustion research facility," J. Propul. Power **11,** 1080–1083 (1995).
37. M. R. Gruber, R. A. Baurle, T. Mathur, and K.-Y. Hsu, "Fundamental studies of cavity-based flameholder concepts for supersonic combustors," J. Propul. Power **17,** 146–153 (2001).
38. M. R. Gruber, J. M. Donbar, C. D. Carter, and K.-Y. Hsu, "Mixing and combustion studies using cavity-based flameholders in a supersonic flow," J. Propul. Power **20,** 769–778 (2004).
39. J. Luque and D. R. Crosley, "LIFbase: Database and Spectral Simulation," SRI International Report MP99-009 (1999), http://www.sri.com/psd/lifbase.
40. C. C. Rasmussen, J. F. Driscoll, C. D. Carter, and K.-Y. Hsu, "Characteristics of cavity-stabilized flames in a supersonic flow," J. Propul. Power **21,** 765–768 (2005).
41. C. P. Gendrich and M. M. Koochesfahani, "A spatial correlation technique for estimating velocity fields using molecular tagging velocimetry (MTV)," Exp. Fluids **22,** 67–77 (1996).
42. R. K. Cohn and M. M. Koochesfahani, "The accuracy of remapping irregularly spaced velocity data onto a regular grid and the computation of vorticity," Exp. Fluids **29,** S61–S69 (2000).
43. R. W. Pitz and J. W. Daily, "Combustion in a turbulent mixing layer formed at a rearward-facing step," AIAA J. **21,** 1565–1570 (1983).